Full-waveform inversion for reservoir characterization: A synthetic study

Nishant Kamath, Ilya Tsvankin & Ehsan Zabihi Naeini

ABSTRACT

Most current reservoir-characterization workflows are based on classic amplitude-variation-with-offset (AVO) inversion techniques. Although these methods have been widely used over the years, full-waveform inversion (FWI) represents a potentially powerful tool for higher-resolution reservoir characterization. An important step in developing reservoir-oriented FWI is the implementation of facies-based rock-physics constraints adopted from the classic methods. We show that such constraints can be incorporated into FWI by adding appropriately designed regularization terms to the objective function. The advantages of the proposed algorithm are demonstrated on both isotropic and VTI (transversely isotropic with a vertical symmetry axis) models with pronounced lateral and vertical heterogeneity. The inversion results are in agreement with published theoretical radiation (scattering) patterns produced by perturbations in the medium parameters.

Key words: Reservoir characterization, VTI, FWI, facies analysis

1 INTRODUCTION

Conventional reservoir-characterization techniques employ amplitude variation with offset (AVO) information and usually operate in the migrated domain. Such "classic" methods invert the AVO response in deterministic or stochastic fashion for elastic or reservoir parameters (Russell, 1988). Coléou et al. (2005) proposed an approach whereby the difference between synthetic gathers, generated for an initial petro-elastic model, and the migrated recorded data is iteratively reduced by model updating. The inversion yields more plausible reservoir parameters by incorporating prior information about geologic facies (Saussus and Sams, 2012). Such information can be included in the form of linear relationships between elastic properties (e.g., between acoustic impedance and density). Such techniques, however, suffer from several inherent problems: the quality of migrated gathers depends on the accuracy of the velocity model, and inversion uses only amplitudes (rather than waveforms).

Full-waveform inversion (FWI) estimates subsurface properties (such as velocity, impedance, etc.) directly from recorded seismic traces. The inverse problem is highly nonlinear and over-determined, yet under-constrained. There are inherent trade-offs between model parameters, which influence the objective function in different ways (Alkhalifah and Plessix, 2014; Kamath and Tsvankin, 2016). Incorporating model constraints sets bounds in the model space and helps obtain more accurate and geologically plausible results (Asnaashari et al., 2013; Duan and Sava, 2016).

In this paper, we incorporate prior information about geologic facies into the FWI objective function. The technique is applied to both isotropic and VTI (transversely isotropic with a vertical symmetry axis) models. The facies-based approach produces superior (compared to the standard FWI) results for isotropic media. In the presence of anisotropy, our method takes advantage of prior information to resolve VTI parameters which are otherwise poorly constrained.

2 METHODOLOGY

FWI is an inversion method that usually operates with raw seismic data (typically shot records) and aims to use the entire waveforms. The output depends on the specific formulation of the problem and study objectives (which also determine the choice of forward modeling) and can include parameters of acoustic or elastic models (which can be isotropic or anisotropic). To apply FWI as a reservoir-characterization tool, one can follow the workflow (Figure 1) discussed by Zabihi Naeini et al. (2016).

In its most general form, FWI is performed by minimizing an objective function which typically represents the l_2-norm of the difference between the modeled and recorded data (i.e., data misfit). Here, we propose to apply model constraints

by including additional terms in the objective function $E(\mathbf{m})$:

$$E(\mathbf{m}) = \|\mathbf{W}_d(\mathbf{d}_m(\mathbf{m}) - \mathbf{d}_o)\|^2 + \beta\|\mathbf{W}_m(\mathbf{m} - \mathbf{m}_c)\|^2$$

$$= E_d(\mathbf{m}) + E_{\text{prior}}(\mathbf{m})\,, \quad (1)$$

where $\mathbf{m}$ is the vector of model parameters, $\mathbf{d}_m(\mathbf{m})$ denotes data generated for model $\mathbf{m}$, $\mathbf{d}_o$ are the observed data, $\mathbf{m}_c$ are the model constraints presumably obtained from well logs, $\mathbf{W}_d$ and $\mathbf{W}_m$ are the data- and model-weighting matrices, respectively, and β determines the relative contribution of prior information.

The first term $[E_d(\mathbf{m})]$ in equation 1 is the data misfit and the second one $[E_{\text{prior}}(\mathbf{m})]$ is the model misfit, which includes rock-physics constraints for each facies. The constraints are in the form of linear relationships between different model parameters. By referring to the "standard" FWI below, we mean the result of minimizing only the data misfit $E_d(\mathbf{m})$ (i.e., $\beta = 0$).

Representative facies are supposed to be identified from well data. We incorporate model constraints $[E_{\text{prior}}(\mathbf{m})]$ into FWI one facies at a time. The gradient of the data misfit with respect to the model parameters is computed from the adjoint-state method (Plessix, 2006; Kamath and Tsvankin, 2016). The bounded, low-memory BFGS (Broyden-Fletcher-Goldfarb-Shanno) algorithm of Byrd et al. (1995) is employed to update the model at each iteration of FWI.

3 NUMERICAL EXPERIMENTS

3.1 Isotropic models

When performing FWI, it is common to first invert diving-wave data in order to update the background velocity model. Here, we show an example of inverting such data for a simple isotropic model with vertical gradients and Gaussian anomalies in the P- and S-wave velocities V_P and V_S (Figure 2). The initial V_P- and V_S-fields (Figures 2(c) and 2(d), respectively) have substantially lower gradients compared to the actual model. P- and S-wave transmission data are influenced by V_P and V_S, respectively (Kamath and Tsvankin, 2016). Hence, in the absence of parameter trade-offs, the inversion algorithm is able to update the velocities and partially recover the anomalies. The inversion results depend on the magnitude of the velocity gradients and offset-to-depth ratios. Note that for the model in Figure 2 the ratio of the maximum offset to the depth of the bottom of the model is close to three.

Once the background velocities have been updated, one can incorporate reflection data to further refine the model. We use a two-facies isotropic model (Figure 3), parameterized in terms of the P-wave acoustic impedance I_P and the P- and S-wave velocities V_P and V_S, to test our algorithm. This choice of parameterization helps avoid the trade-off between V_P and density ρ for short-offset P-wave reflection data (Operto et al., 2013). Parameterizing the model in terms of I_P, V_P, and V_S ensures that there is no trade-off between the P-wave velocity and the other parameters. The initial model is obtained by smoothing the actual impedance and velocity fields.

At the first stage of inversion, we constrain the velocities V_P and V_S by honoring the ratios I_P/V_P and I_P/V_S (assumed to be known *a priori*) in the first layer throughout the model (Figure 4). The output of this stage is then used as the initial model for the next stage, in which model constraints (the same ratios as before) are imposed only on the second layer. This is done by applying a model mask designed based on the results of the first stage (Figure 5). In addition, at the second stage we include higher temporal frequencies in the data. The results obtained by our facies-based approach are superior to those of the standard FWI (Figure 6).

For our next experiment, we use an isotropic model which includes a laterally hererogeneous, thin reservoir located at a depth of 1.6 km beneath a stratified overburden (Figure 7). The lateral variation of the elastic properties within the reservoir is caused by interchanging oil, gas, and brine sands. The facies encasing the reservoir represents shale; there is a total of three nonreservoir facies in the model.

As before, we proceed in two stages: first, the I_P/V_P and I_P/V_S ratios for the shale facies are employed as constraints for depths between 1.1 and 2.3 km. The mask used to impose the constraints is depicted in Figure 8(a). The results of this stage are used as the input for the next one, in which the constraints are applied just to the reservoir facies.

Starting from the initial model in Figures 7(a) $-$ 7(c), the standard FWI produces the I_P- and V_P-fields with artifacts in the shale facies (Figure 9). In addition, the reservoir layer is not sufficiently well resolved. The shale parameters obtained from the first stage of our facies-based inversion are more consistent with the actual model. The reservoir layer, however, exhibits artifacts similar to those in the standard FWI. The second stage of the facies-based inversion mitigates these distortions, especially in the I_P- and V_P-fields. The density values computed from the inverted acoustic impedance and P-wave velocities are not sufficiently accurate. This is most likely because the inverted I_P-field has a higher vertical resolution compared to that of the velocity V_P.

3.2 VTI model

It is generally well recognized that reservoir-oriented FWI has to take anisotropy into account (Zabihi Naeini et al., 2016). We extend the proposed method to elastic VTI media as the first step towards incorporating realistic anisotropic symmetries. The parameterization includes V_{hor} (the P-wave horizontal velocity), V_{S0} (the S-wave vertical velocity), and the anisotropy coefficients ϵ and $\eta \equiv (\epsilon - \delta)/(1 + 2\delta)$. This choice, suggested by radiation-pattern analysis (Alkhalifah and Plessix, 2014; Kamath et al., 2016), optimizes the inversion by reducing parameter trade-offs.

The VTI model in Figure 10 has the same vertical velocities V_{P0} and V_{S0} and density as the isotropic model in Figure 7. However, we consider the encasing shale to be VTI, while the reservoir sand is isotropic, which helps differentiate between them in the inversion. Because we were unable to

properly update the density for the isotropic model, the actual density field is smoothed and kept fixed during the inversion. The smoothing filter employed to generate the initial velocity models is also used to obtain the initial anisotropy parameters and the density.

We invert for the four model parameters ($V_{\rm hor}$, V_{S0}, η, and ϵ) using both the standard FWI and our facies-based approach (Figure 11). The latter is implemented by imposing "isotropic" constraints (i.e., penalizing nonzero values of η) on the reservoir. The velocities V_{P0} (obtained from the inverted $V_{\rm hor}$ and ϵ using the relationship $V_{\rm hor} = V_{P0}\sqrt{1+2\epsilon}$) and V_{S0} are generally well constrained; our facies-based approach leads to a slight improvement over the standard FWI inside the reservoir. The coefficient ϵ is also accurately estimated by both methods with positive values for the shale, whereas the reservoir is practically isotropic ($\epsilon \approx 0$). For the chosen parameterization the objective function is weakly sensitive to the anellipticity coefficient η (Kamath et al., 2016), and the standard FWI is unable to resolve this parameter (Figure 11(c)). The facies-based approach, however, produces a sufficiently accurate estimate of η (Figure 11(g)).

4 CONCLUSIONS

With the goal of extending FWI to reservoir characterization, we introduced a practical approach to add facies-based rock-physics constraints through regularization terms in the objective function. The method was first tested on a simple isotropic model that includes two facies and is parameterized in terms of the acoustic impedance I_P and the P- and S-wave velocities V_P and V_S. Imposing facies-based constraints during the inversion mitigates artifacts in I_P and improves the resolution in this parameter.

The second model consists of four facies, one of which represents the reservoir. Our algorithm produced more accurate results for the facies encasing the reservoir compared with the standard FWI and improved the resolution in the reservoir parameters.

In another test, we introduced anisotropy in the facies encasing the reservoir (shale). The algorithm updated the P-wave horizontal velocity $V_{\rm hor}$, the S-wave vertical velocity V_{S0}, and the anisotropy coefficients η and ϵ, while the density field, obtained by smoothing the actual model, was kept fixed. For the chosen parameterization, the objective function is not sufficiently sensitive to η. The facies-based approach succeeded in steering the inversion closer to the actual η-values by imposing appropriate constraints. Including anisotropy may represent an advantage (depending on the availability of parameter relationships) for the facies-based algorithm because there are more degrees of freedom in classifying the facies and constraining the inversion.

REFERENCES

Alkhalifah, T., and R. Plessix, 2014, A recipe for practical full-waveform inversion in anisotropic media: An analytical parameter resolution study: Geophysics, **79**, R91–R101.

Asnaashari, A., R. Brossier, S. Garambois, F. Audebert, P. Thore, and J. Virieux, 2013, Regularized seismic full waveform inversion with prior model information: Geophysics, **78**, R25–R36.

Byrd, R. H., P. Lu, J. Nocedal, and C. Zhu, 1995, A limited memory algorithm for bound constrained optimization: SIAM Journal on Scientific Computing, **16**, 1190–1208.

Coléou, T., F. Allo, R. Bornard, J. Hamman, and D. Caldwell, 2005, Petrophysical seismic inversion: SEG Technical Program Expanded Abstracts 2005, 1355–1358.

Duan, Y., and P. Sava, 2016, Elastic wavefield tomography with physical model constraints: Geopysics, **81**, R447–R456.

Kamath, N., and I. Tsvankin, 2016, Elastic full-waveform inversion for VTI media: Methodology and sensitivity analysis: Geophysics, **81**, C53–C68.

Kamath, N., I. Tsvankin, and E. Díaz, 2016, Elastic FWI for VTI media: A synthetic parameterization study: SEG Technical Program Expanded Abstracts, 301–305.

Operto, S., Y. Gholami, V. Prieux, A. Ribodetti, R. Brossier, L. Metivier, and J. Virieux, 2013, A guided tour of multiparameter full-waveform inversion with multicomponent data: From theory to practice: The Leading Edge, **32**, 1040–1054.

Plessix, R., 2006, A review of the adjointstate method for computing the gradient of a functional with geophysical applications: Geophysical Journal International, **167**, 495–503.

Russell, B. H., 1988, Introduction to seismic inversion methods: Society of Exploration Geophysicists.

Saussus, D., and M. Sams, 2012, Facies as the key to using seismic inversion for modelling reservoir properties: First Break, **30**, 45–52.

Zabihi Naeini, E., T. Alkhalifah, I. Tsvankin, N. Kamath, and J. Cheng, 2016, Main components of full-waveform inversion for reservoir characterization: First Break, **34**, 37–48.

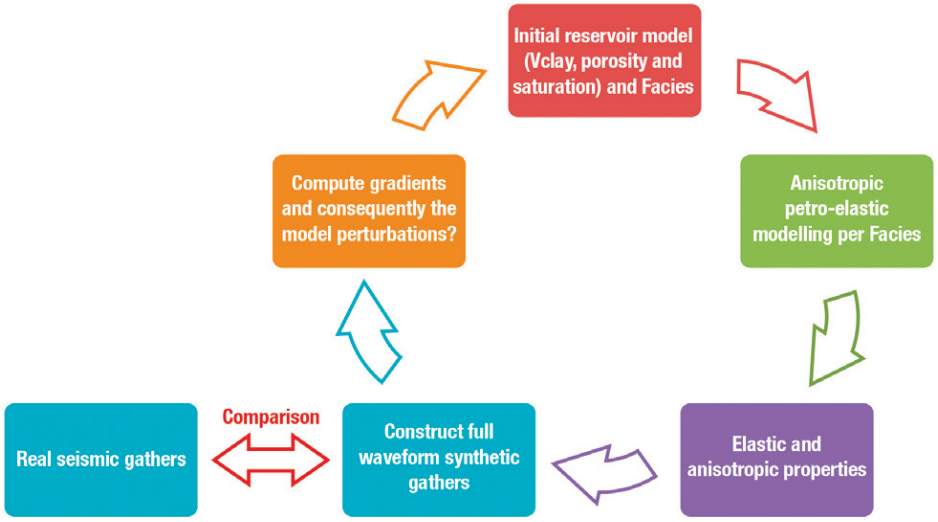

Figure 1. Concept diagram for anisotropic elastic reservoir-oriented FWI (Zabihi Naeini et al., 2016).

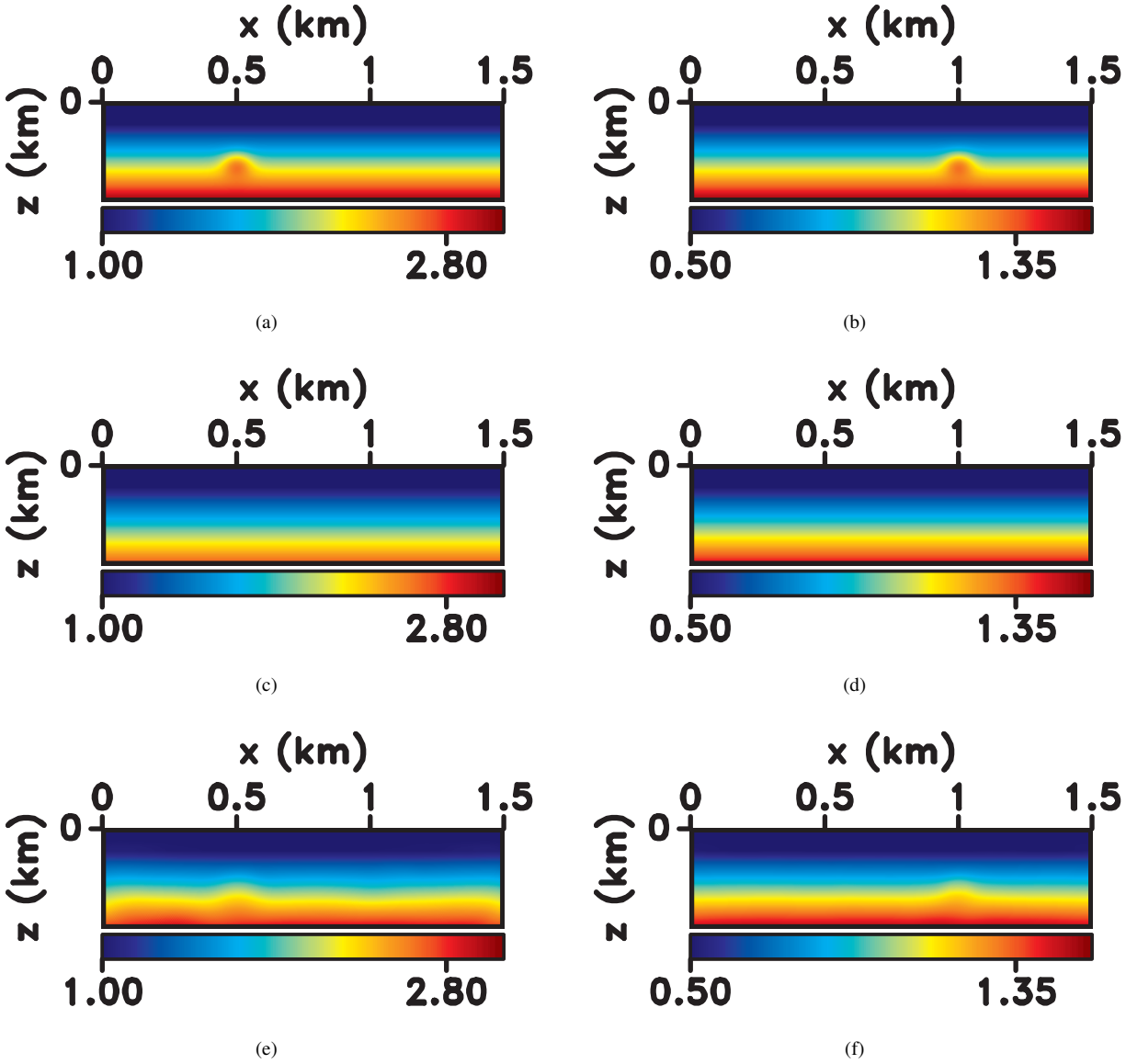

Figure 2. Elastic isotropic FWI of diving P- and SV-waves. The actual velocities (a) V_P and (b) V_S, the initial (c) V_P and (d) V_S, and the inverted (e) V_P and (f) V_S. The velocities here and in the subsequent plots are in km/s.

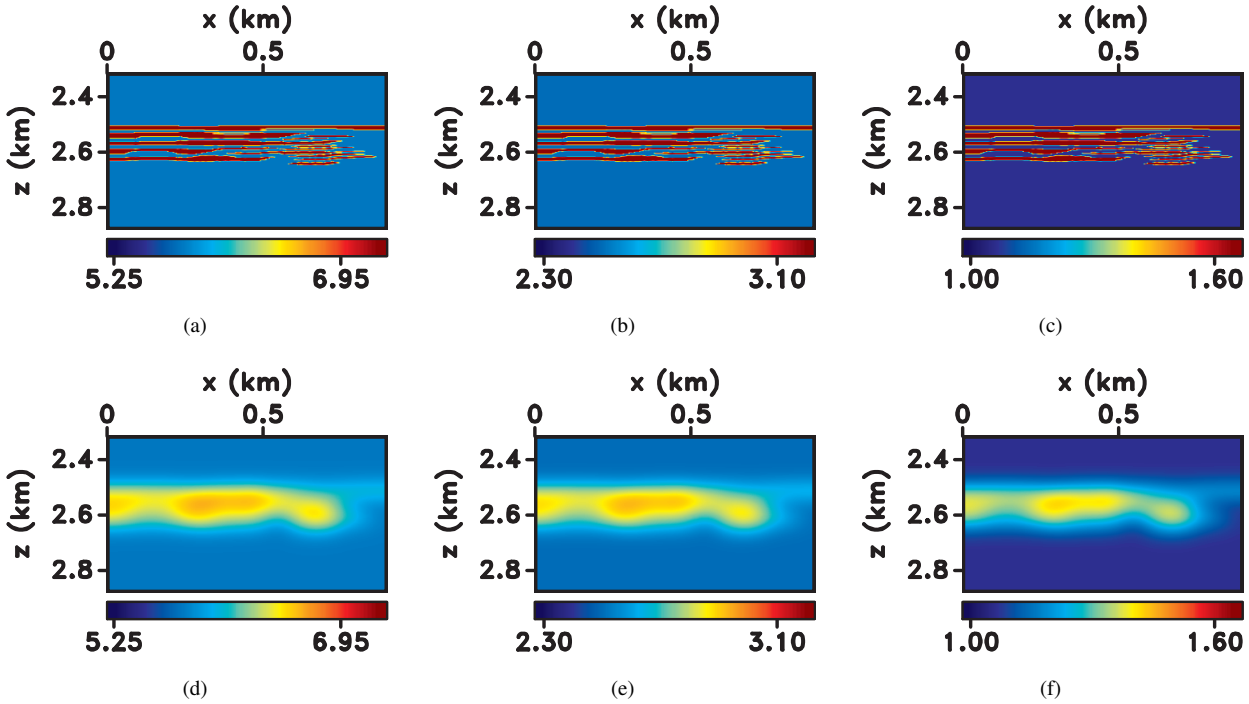

Figure 3. Two-facies isotropic model employed to test the proposed FWI algorithm. The actual impedance (a) I_P and the velocities (b) V_P and (c) V_S. The initial parameters (d) I_P, (e) V_P, and (f) V_S. The P-wave impedance is in $10^{-6}\mathrm{kg}/(\mathrm{m}^2\mathrm{s})$.

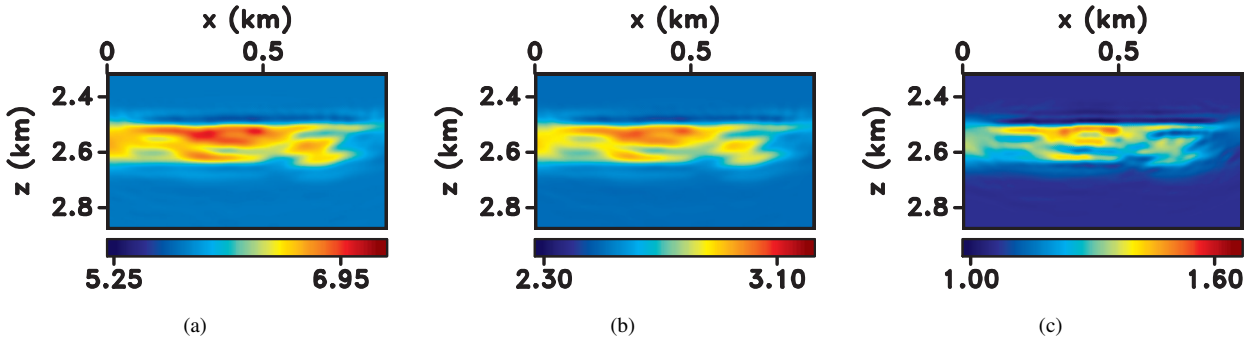

Figure 4. Results of the first stage of the facies-based FWI. The inverted parameters (a) I_P, (b) V_P, and (c) V_S.

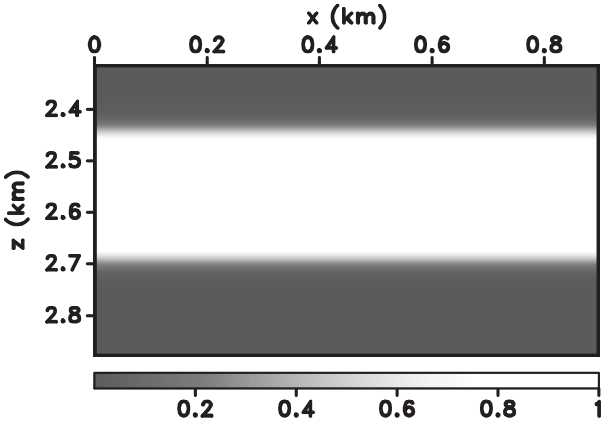

Figure 5. Mask used in the facies-based FWI for the model from Figure 3.

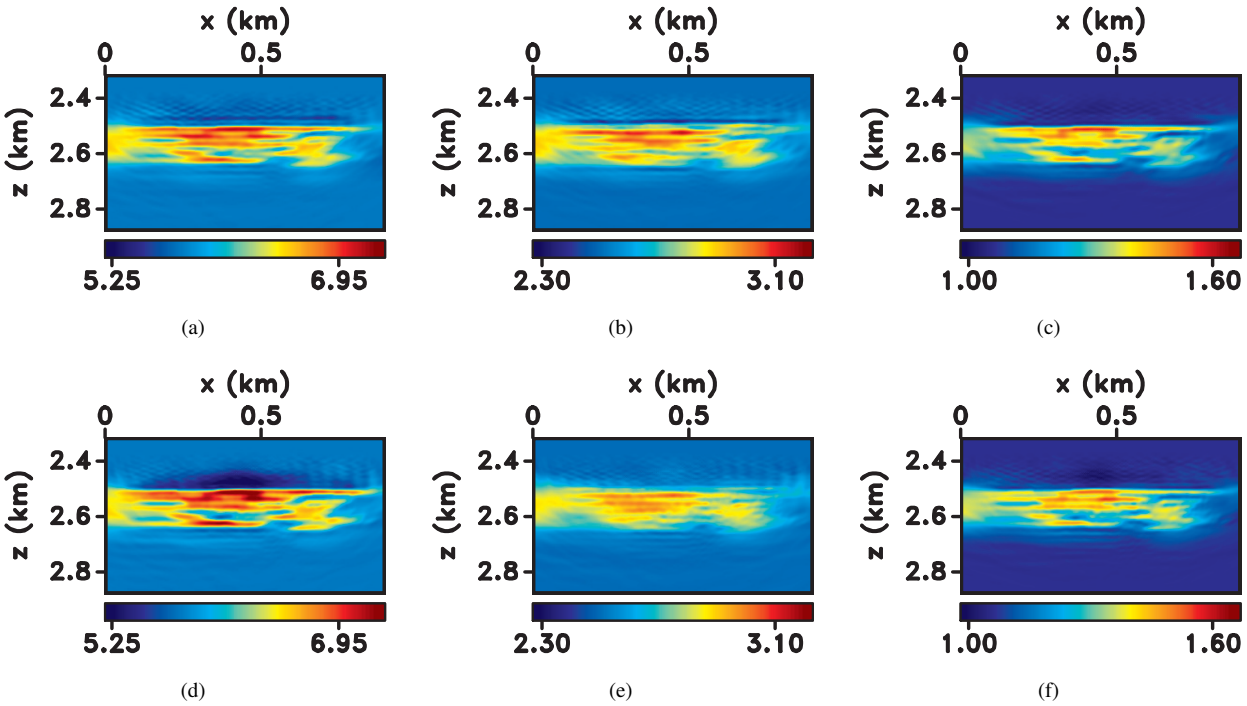

Figure 6. Parameters (a) I_P, (b) V_P, and (c) V_S of the model from Figure 3 obtained from the second stage of the facies-based FWI. The (d) I_P-, (e) V_P-, and (f) V_S-fields from the standard FWI.

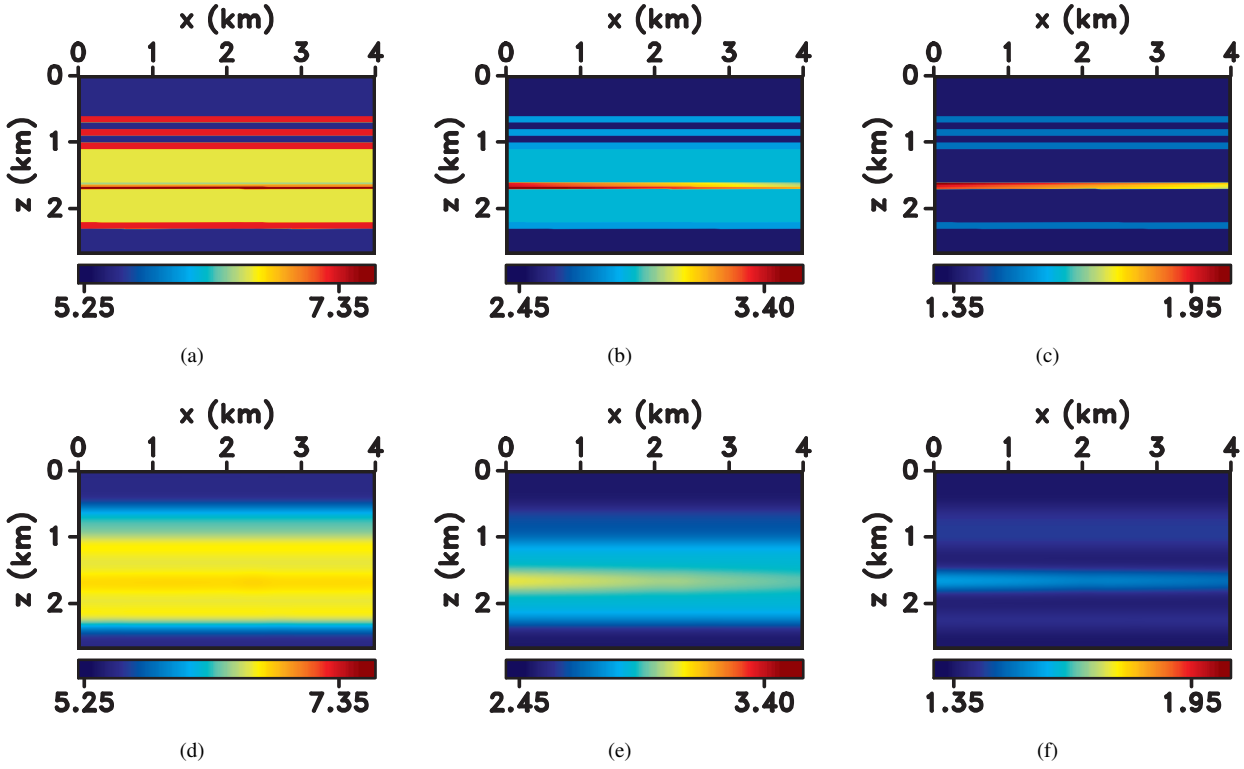

Figure 7. Elastic isotropic model described by the (a) acoustic impedance (AI) and the velocities (b) V_P and (c) V_S. The initial parameters (d) AI, (e) V_P, and (f) V_S.

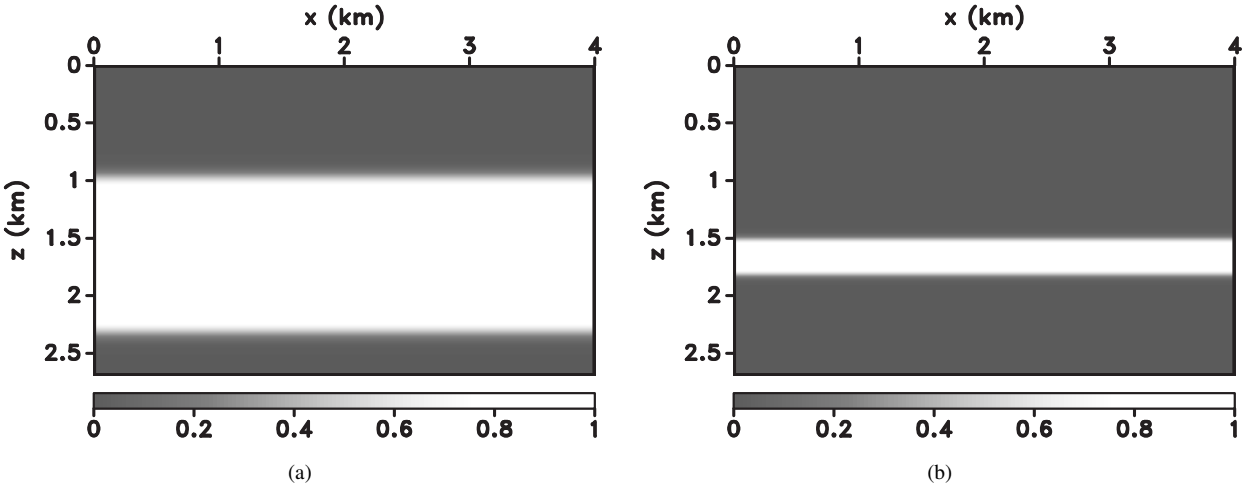

Figure 8. Masks for the model in Figure 7 used in the (a) first and (b) second stages of the facies-based FWI.

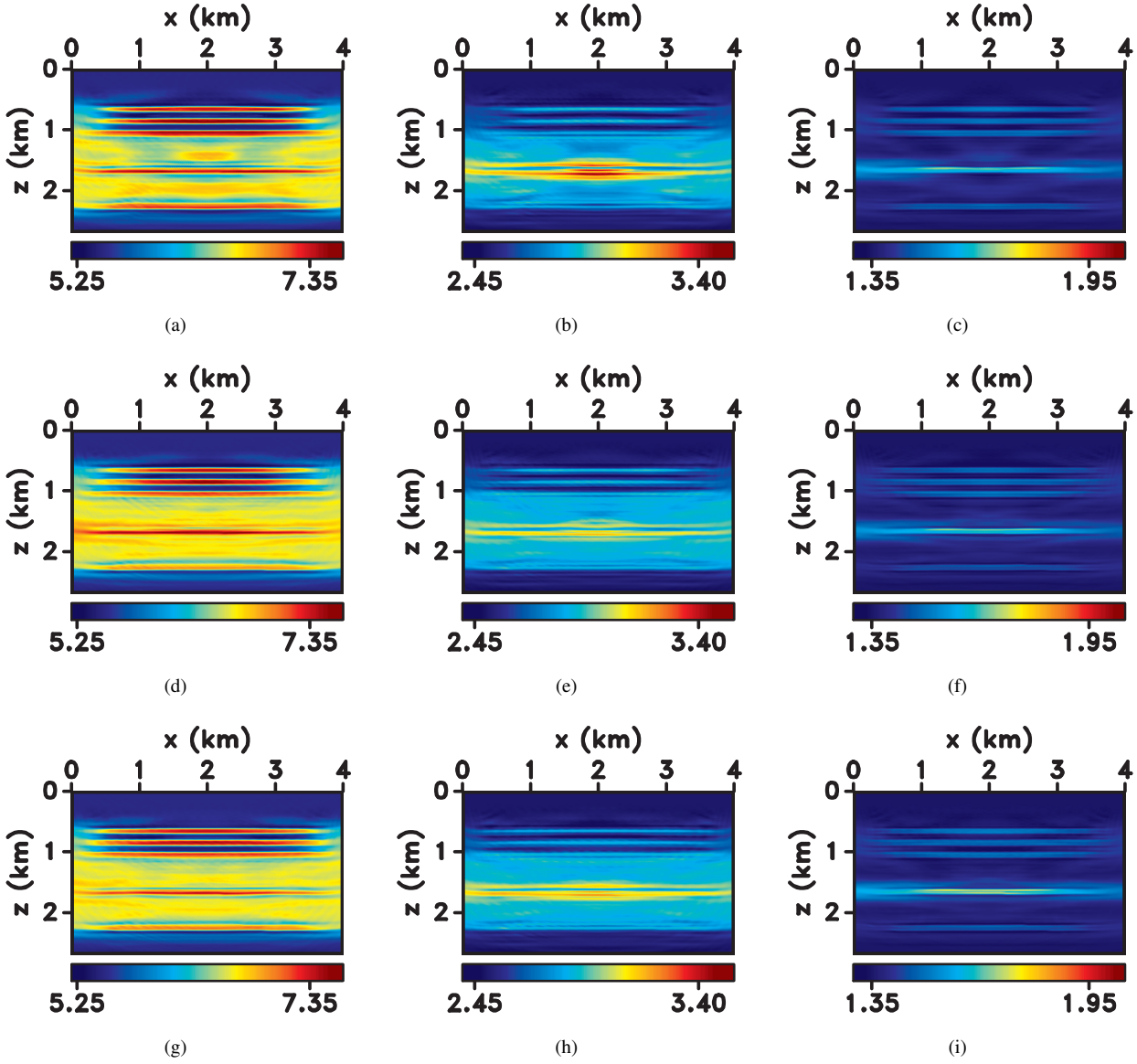

Figure 9. (a) Acoustic impedance I_P and the velocities (b) V_P and (c) V_S for the model from Figure 7 obtained from the standard FWI. The parameters (d) I_P, (e) V_P, and V_S after stage I of the facies-based FWI. The (g) I_P-, (h) V_P-, and (i) V_S-fields after stage II of the facies-based FWI.

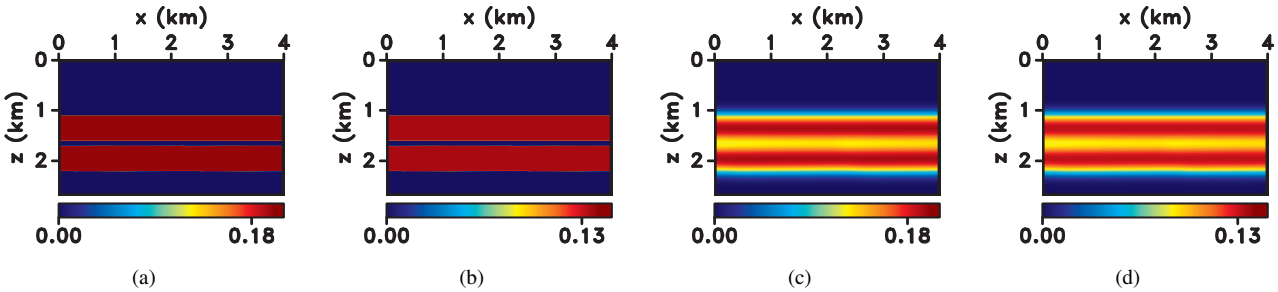

Figure 10. Anisotropy parameters (a) ϵ and (b) η of an elastic VTI model. The initial parameters (c) ϵ and (d) η. The P- and S-wave vertical velocities (V_{P0} and V_{S0}) are the same as V_P and V_S for the isotropic model in Figure 7.

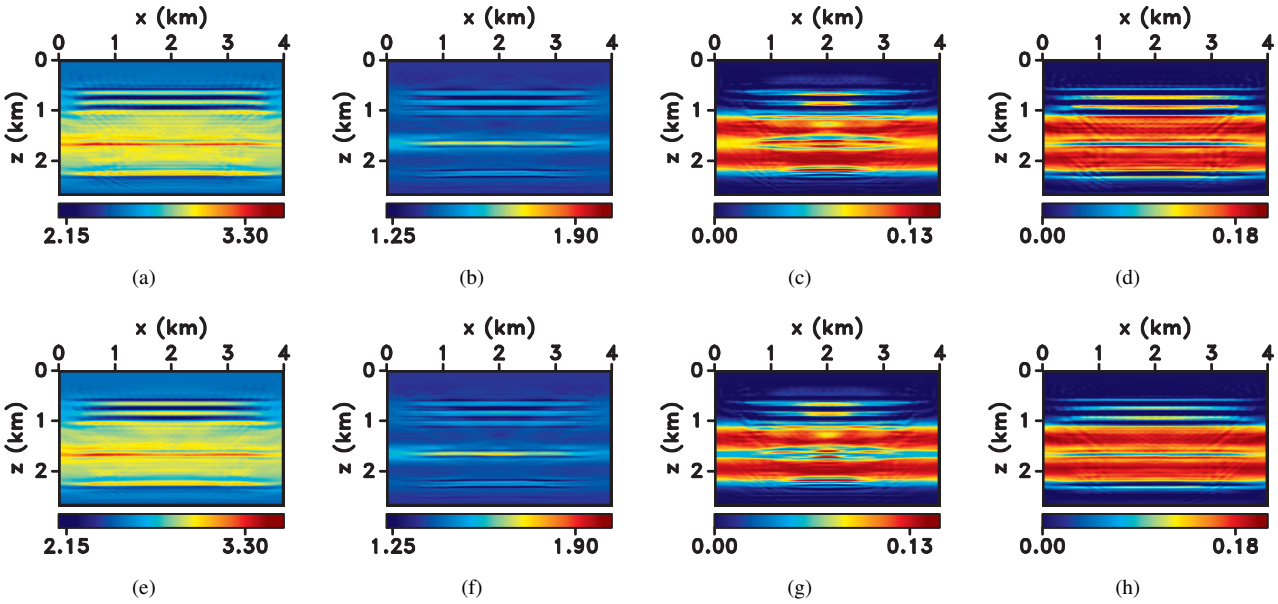

Figure 11. VTI parameters (a) V_{P0}, (b) V_{S0}, (c) η, and (d) ϵ obtained from the standard FWI. The parameters (e) V_{P0}, (f) V_{S0}, (g) η, and (h) ϵ obtained from the facies-based FWI.